Nucleation Kinetics, Size Effects, and Surface Treatment

10

Toshio Takiya, Karin Furukawa, Naoaki Fukuda, Min Han, and Minoru Yaga

Contents

Abstract

The rate equations that describe nanoparticle formation have been derived on the basis of kinetic theory and statistical thermodynamics. In the formation

T. Takiya (✉) • K. Furukawa
Hitachi Zosen Corporation, Osaka, Japan
e-mail: takiya@hitachizosen.co.jp; karin@hitachizosen.co.jp

N. Fukuda
Office of Society-Academia Collaboration for Innovation, Kyoto University, Kyoto, Japan
e-mail: fukuda.naoaki.7v@kyoto-u.ac.jp

M. Han
Department of Materials Science and Engineering, Nanjing University, Nanjing, China
e-mail: sjhanmin@nju.edu.cn

M. Yaga
Faculty of Engineering, University of the Ryukyus, Okinawa, Japan
e-mail: yaga@tec.u-ryukyu.ac.jp

M. Aliofkhazraei (ed.), *Handbook of Nanoparticles*,
DOI 10.1007/978-3-319-15338-4_15

processes, the critical size of the nucleus of the nanoparticle can be determined to be the nucleus generated under near-equilibrium conditions. Nanoparticles larger than the critical size can continue to grow; nanoparticles smaller than the critical size may become smaller by evaporation. However, under strongly nonequilibrium conditions such as the supersonic expansion of a neutral gas, the concept of a critical nucleus becomes irrelevant because the calculated critical size becomes smaller than the atomic diameter. Consideration of very small clusters from a kinetic standpoint is very important for understanding the early stages of nanoparticle formation under nonequilibrium conditions. In the present chapter, the rate equations that describe condensation and evaporation during nanoparticle formation and growth are described using molecular partition functions based on statistical thermodynamics. The equations are used to determine nanoparticle size, which accounts for the characteristics of the materials. The effects of size and surface treatment of nanoparticles are also described, the objective being practical application of this information.

Keywords
Nanoparticle formation • nanoparticle size • size distribution • nanocoating • nanocomposite • kinetic theory • statistical thermodynamics • nonequilibrium phenomena • heterogeneous nucleation

Introduction

Nanometer-sized particles, or nanoparticles, are assemblies composed of up to several tens of thousands of atoms or molecules, most of which are located on or near the surface of the nanoparticles. The structure of nanoparticles is responsible for the fact that they have characteristics substantially different from bulk materials in the gas, liquid, or solid phases [1]. Furthermore, because of the small size of nanoparticles, thermal or quantum fluctuations, which have never been observed in macroscopic systems, become an important factor in determining the dynamics of the nanoparticles. The discrete nature of electronic energy levels leads to the emergence of anomalous specific heat, thermal, chemical, and magnetic properties even at room temperature [2]. The appearance of new absorption bands in the range of the near infrared and the far infrared is a phenomenon different from bulk materials. Due to peculiar quantum and surface effects, nanoparticles possess great potential to exhibit new, useful properties. Highly functional devices synthesized from nanoparticles have been studied for use in various fields, such as semiconductors [3], photocatalysis [4], gas sensors [5–7], secondary batteries [8–10], superconductors [11], and bonding substances [12, 13].

There are two broad categories of methods for creating nanoparticles: gas-phase and liquid-phase method. Cooling occurs during expansion of a vapor

evaporated from a solid surface by mechanisms such as gas evaporation [14], arc discharge [15], magnetron sputtering [16, 17], plasma deposition processes [18], and pulsed laser ablation [19–21]. In contrast, coprecipitation processes [22], sol–gel processes [23], reduction processes [24], and hydrothermal synthesis processes [25] are possible ways of controlling the size of nanoparticles in the liquid phase.

Use of nanoparticles in a semiconductor device or a chemical sensor is widely expected to facilitate the application of quantum effects. The size of the nanoparticles greatly influences the onset of the effects and is therefore a very important consideration in the synthesis of nanoparticles. Understanding the process of nanoparticle formation with an adequate physical model is necessary for size control. In the conventional droplet model, the number density and particle size are determined on the basis of growth equations after calculating the critical conditions for nucleation [26]. Although the droplet model method has produced many successful results [27, 28], some cases have also been incompatible with the model. In these cases the critical nuclei become very small under strongly nonequilibrium conditions [29]. In such cases, the nanoparticle size and number density must be calculated at an early stage, and kinetic theory must be used to take into consideration dimer formation [30].

In the present chapter, kinetic theory will be used to describe the mechanism of nanoparticle formation. The description will enable the reader to understand what controls the size of nanoparticles and to make use of the size effect. Whereas the rate equations for nanoparticle formation are expressed by statistical mechanics in the kinetic theory, a molecular partition function will assume a large role in the process described here. In section "Kinetics of Nanoparticle Formation" of the chapter, the kinetics and statistical thermodynamics needed to formulate the phenomenon and to compare the process with classical nucleation were reviewed. After providing analytical methods and models for making calculations, an example of nanoparticle formation, the options for controlling size, and an illustration of size effects were presented in section "Size Effect of Nanoparticles." Surface coating and surface modification of relevance to industrial applications will be introduced in section "Surface Treatment of Nanoparticles." Finally, conclusions are given in section "Conclusion."

Kinetics of Nanoparticle Formation

In this section, a physical model related to the generation and growth of nanoparticles will be explained in detail, and the assumptions of the model will be scrutinized. The work may prove to be useful for improvement and reconstruction of the physical model and, by extension, may eventually contribute to the design of a device for generating and classifying nanoparticles for industrial use.

Dynamics of Cluster Behavior

Nanoparticle formation is based on an equilibrium phase transition that involves atomic or molecular condensation, but at an early stage of the formation process, nonequilibrium phenomena possibly occur. Here, a cluster is defined as an assembly of atoms or molecules before a stable nanoparticle forms. Because cluster generation or nucleation at an early stage of the process will determine the characteristics of the nanoparticles that are produced, it is very important to understand the dynamics of clusters.

The following equations characterize reactions that allow for every possible pathway for the generation and growth of atomic clusters [31]:

$$A + A_n \rightarrow A_{n+1}\ (\text{condensation}) \tag{1}$$

$$A_{n+1} \rightarrow A_n + A\ (\text{evaporation}) \tag{2}$$

$$A_m + A_n \rightarrow A_{m+n}\ (\text{coagulation}) \tag{3}$$

$$A_m \rightarrow A_{m-n} + A_n\ (\text{collapse}) \tag{4}$$

$$2A + M \rightarrow A_2 + M\ (\text{three} - \text{body attachment}) \tag{5}$$

$$A_2 + M \rightarrow 2A + M\ (\text{dissociation}) \tag{6}$$

Here, the symbol A represents a monatomic molecule or a monomer, A_n is a cluster consisting of n-monomers (referred to as an "n-cluster"), and M is a molecule of a carrier gas. The rate equations corresponding to the above reactions will be described below. First, the equation for the rate of change of the number density (Z_1) of the monomer is expressed as follows:

$$\frac{dZ_1}{dt} = -Z_1 \sum_{m=2}^{N} Z_m k_{1,m} + \sum_{m=3}^{N} Z_m \nu_{m-1,1} - 2Z_1^2 Z_b k_{att} + 2Z_2 Z_b \nu_{dis} \tag{7}$$

Here, the symbol Z_m is the number density of a cluster consisting of m-monomers, Z_b is the number density of molecules of carrier gas, and $\nu_{m-1,1}$, $k_{1,m}$, k_{att}, and ν_{dis} are the rate constants for evaporation, condensation, three-body attachment, and three-body dissociation, respectively. The number N is the maximum size of clusters within the system. The equation for the rate of change of the dimer is similarly expressed as follows:

$$\begin{aligned} \frac{dZ_2}{dt} = &-Z_2^2 k_{22} - Z_2 \sum_{m=1}^{N} Z_m k_{2m} \\ &+ Z_4 \nu_{22} + \sum_{m=3}^{N} Z_m \nu_{m-2,2} + Z_1^2 Z_b k_{att} - Z_2 Z_b \nu_{dis} \end{aligned} \tag{8}$$

Furthermore, the generalized rate equation for the cluster consisting of three or more molecules is derived as follows:

$$\frac{dZ_n}{dt} = \sum_{m=1}^{n\geq 2m} Z_{n-m} Z_m k_{n-m,m} - \sum_{m=1}^{n\geq 2m} Z_n v_{n-m,m} - Z_n \sum_{m=1}^{N} (1+\delta_{nm}) Z_m k_{n,m} + \sum_{m=n+1}^{N} \left(1+\delta_{n,m-n}\right) Z_m v_{n,m-n} \tag{9}$$

In Eq. 9, the first and the third terms on the right-hand side represent an increase by condensation and a decrease of n-clusters by coagulation, respectively. The second and fourth terms likewise represent a decrease by evaporation and an increase by collapse, respectively. Here, δ_{ij} is the Kronecker delta; in Eq. 9, it enables double counting of the creation and annihilation of n-clusters when clusters of the same size interact with each other.

To use the above-derived equations to calculate the number density associated with cluster formation, the unknown constants that appear in Eqs. 7, 8, and 9 must be determined. The method of determination will be described in the following sections.

Equation for Rate of Change of Critical Nuclei in the Liquid Droplet Model

In the liquid droplet model, the nucleation and growth of the atomic cluster can be described as if the cluster has a completely spherical body, as shown in Fig. 1.

It may be supposed in Fig. 1 that the growth of a cluster could be based on attachment and detachment of only one molecule. In other words, if Z_n is the number density of n-clusters, the rate of change of Z_n is expressed by

$$\frac{dZ_n}{dt} = J_{n-1} - J_n \qquad (\text{change} = \text{arrivals at } n - \text{departures from } n) \tag{10}$$

In Eq. 10, J_n is the net flux of n-clusters that change into $(n+1)$ clusters and can be expressed by the following equation:

$$J_n = f_n Z_n - g_{n+1} Z_{n+1} \qquad (\text{net flux} = \text{visits} - \text{returns}) \tag{11}$$

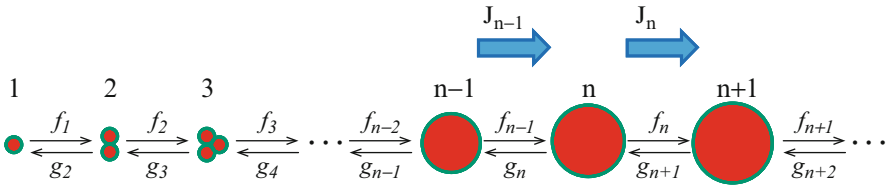

Fig. 1 Liquid droplet model of cluster growth

Here, f_n is the rate of attachment of one molecule onto the n-cluster, corresponding to $Z_1 k_{n,1}$ in Eq. 9, with dimensions of inverse time. Also, in a similar way, g_n is the rate of detachment of one molecule from the n-cluster, corresponding to $v_{n-1,1}$ in Eq. 9. The solution for f_i and g_i can be derived by using mathematical induction to expand Eq. 11 and then omitting the terms involving Z_2 to Z_n. If it can be assumed that the net flux of cluster generation is constant, then the following steady condition is true:

$$J_1 = J_2 = \ldots = J_n \equiv J \qquad \left(\frac{dZ_n}{dt} = J_{n-1} - J_n \equiv 0\right) \tag{12}$$

If the variable Z_i^e indicates the equilibrium number density of i-clusters, then Eq. 11 becomes the following expression:

$$f_n Z_n^e - g_{n+1} Z_{n+1}^e = 0 \tag{13}$$

By using Eq. 13, the variables g_i ($i = 1$ to n) in the solution obtained from Eq. 11, can be eliminated and the following equation was obtained:

$$J = \frac{Z_1}{Z_1^e}\left(\frac{1}{f_1 Z_1^e} + \frac{1}{f_2 Z_2^e} + \ldots + \frac{1}{f_n Z_n^e}\right)^{-1} = \frac{Z_1}{Z_1^e}\left(\int_1^n \frac{dk}{f_k Z_k^e}\right)^{-1} \tag{14}$$

To obtain the equilibrium number density of n-clusters, Z_n^e, the energy balance between a multiparticle system and a cluster must then be considered. In a system consisting of n isolated molecules and one n-cluster (Fig. 2) in energy states F_1 and F_n, respectively, the energy states can be expressed by using molecular partition functions.

The equilibrium condition of the n-cluster formed from n isolated molecules is represented by the following equation:

$$\frac{Z_n^e}{Z_1^e} = \exp\left(-\frac{\Delta G_n}{kT}\right) \tag{15}$$

Here, k is Boltzmann constant, T is temperature of the intended system, and the variable ΔG_n is the Gibbs free energy change associated with the formation of the n-cluster and is expressed by the following equation:

$$\Delta G_n = kT \ln\left(\frac{Q_1}{Z_1^e}\right)^n - kT \ln\left(\frac{Q_n}{Z_1^e}\right) \tag{16}$$

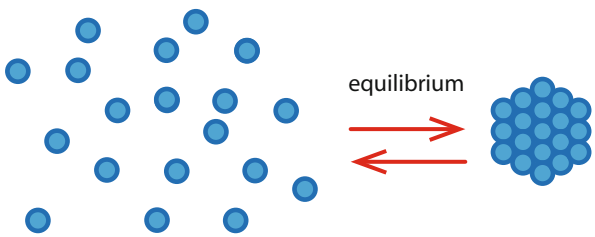

Fig. 2 One n-cluster (*right*) and n isolated molecules (*left*)

Here, Q_i is the molecular partition function of i-cluster and occupies a crucial role in considering nucleation and growth of cluster. Therefore, evaluation of Eq. 16 would be necessary to obtain the equilibrium number density, Z_n^e. For that calculation, the value of the molecular partition function of an n-cluster must be determined on the basis of statistical thermodynamics.

When the solutions of the normal vibrations and rotational inertia of the partition function in Eq. 16 have been obtained, the equations of nucleation and growth can be set into a system of equations of macroscopic processes by using the solutions. However, there is a simplified method that does not involve evaluating the molecular partition functions. Instead, the energies are rewritten in terms of the chemical potential, μ_1, of isolated molecules and the Gibbs free energy of the n-cluster, G_n:

$$\Delta G_n = -n\mu_1 + G_n \tag{17}$$

With respect to the Gibbs free energy G_n, there is a variety of liquid drop models. McClurg [32] has organized the various models in a general formula for G_n:

$$G_n = \alpha_1 n + \alpha_2 n^{2/3} + \alpha_3 n^{1/3} + \alpha_4 \ln(n) + \sum_{i=5}^{\infty} \alpha_5 n^{(5-i)/3} \tag{18}$$

In Eq. 18, the constants of α_1, α_2, α_3, α_4, and α_5 are each determined in a way that is consistent with each model. The explanation of each variable and constant in Eq. 18 is found in the original article, which can be found at the end of this chapter. Under the capillary assumption, an expression involving the potential of bulk state, μ_b, and the surface tension of the cluster, σ, can be used instead of G_n in Eq. 17:

$$\Delta G_n = -n\mu_1 + n\mu_b + 4\pi r^2 \sigma = -n\Delta\mu + a\sigma n^{2/3} \tag{19}$$

Here, $\Delta\mu$ represents the difference between μ_1 and μ_b, r is the radius of a cluster, and $a = (36\pi v^2)^{1/3}$ was eventually set, with v representing the volume of one molecule. In Eq. 19, the value of ΔG_n will first increase as the number of molecules (n) constituting the cluster increases, but the value of ΔG_n will begin to decrease after reaching a peak when the effect of the chemical potential difference becomes larger than that of the surface free energy. The critical value is obtained by differentiating Eq. 19 with respect to n and setting the derivative to zero. The number of molecules n_c at the critical point is

$$n_c = \frac{32}{3}\pi v^2 \left(\frac{\sigma}{\Delta\mu}\right)^3 \tag{20}$$

If ΔG_c indicates the Gibbs free energy associated with formation of the critical cluster, the equilibrium number density of the critical size of the cluster is represented by the following equation:

$$Z_{n_c}^e = Z_1^e \exp\left(-\frac{\Delta G_c}{kT}\right) \tag{21}$$

When the critical size is large, the summation of the series in Eq. 14 can be estimated by an integral, as indicated on the right-hand side of Eq. 14. The equilibrium solution for the critical nucleus generation rate is as follows:

$$J = K_{Zel} f_{n_c} Z_1^e \exp\left(-\frac{\Delta G_c}{kT}\right) \tag{22}$$

Here, K_{Zel} is generally called the *Zel'dovich factor*, which is expressed as follows [33]:

$$K_{Zel} = \sqrt{-\frac{1}{2\pi kT}\left(\frac{\partial^2 \Delta G_n^e}{\partial n^2}\right)_{n=n_c}} \tag{23}$$

The flux J represents the number of critical nuclei generated one unit of volume per unit time and is expressed in an explicit form that can be incorporated into macroscopic equations (e.g., fluid dynamics equations). Equation 22, which was derived from the theory of steady-state transition and equilibrium processes, provides a way to estimate the flux of critical nuclei, and there is still the unknown constant f_n to be determined when $n = n_c$. In the next section, Eyring's transition-state theory [34] will be used to evaluate the rate constant f_n.

The Rate Equation of Cluster Growth

Cluster growth is considered by applying Eyring's transition-state theory. When an n-cluster interacts with a monomer, it may become an $(n + 1)$ cluster through an activated complex A_{n+1}^*. The process can be represented by the following equation:

$$A_1 + A_n \leftrightarrow A_{n+1}^* \rightarrow A_{n+1} \tag{24}$$

As well known in the theory, there is an equilibrium relationship between the original system and the product system A_{n+1}^*, which is represented by using the equilibrium constant K_{n+1}^* in the following equation [35]:

$$K_{n+1}^* = \frac{Q_{n+1}^*}{Q_1 Q_n} \exp\left(\frac{D^*}{kT}\right) \tag{25}$$

Here, Q_{n+1}^* is the molecular partition function of the activated complex, and D^* is the dissociation energy associated with detachment of one monomer from the complex. By introducing a critical state of the activated complex indicated with Q_{n+1}^+, we obtain the rate constant f_n as follows [35]:

$$f_n = \frac{kT}{h} \frac{Q_{n+1}^+}{Q_1 Q_n} Z_1 \exp\left(-\frac{\Delta E}{kT}\right) \tag{26}$$

Here, h is Planck constant, and ΔE is the activation energy that the reaction has to overcome to become an $(n+1)$ cluster. If we collect the variables into a constant ξ_n, a style of equation familiar in kinetic theory is obtained as follows:

$$f_n = \xi_n \frac{P_1}{(2\pi mkT)^{1/2}} an^{2/3} \tag{27}$$

where P_1 and m are the pressure and the mass of monomer, respectively. The rate constant of evaporation can be derived from Eqs. 13 and 15 as follows:

$$g_{n+1} = \frac{Z_n^e}{Z_{n+1}^e} f_n = \xi_n \frac{P_1}{(2\pi mkT)^{1/2}} an^{2/3} \exp\left(\frac{\partial \Delta G_n}{\partial n}\right) \tag{28}$$

When the derived rate equations, Eqs. 27 and 28, are substituted into Eq. 11, the number density of each size cluster can be determined, and that leads to the solution for nanoparticle formation.

Size Effect of Nanoparticles

In the previous section, the mechanism of nanoparticle formation has been described to enhance understanding of phenomena related to control of nanoparticle size and to facilitate application to actual industrial problems. In the following part of this chapter, some practical examples concerning the effects of nanoparticle size and ways of controlling the size will be introduced.

Synthesizing Size-Selected Nanoparticles

The methods for synthesizing nanoparticles are classified as gas-phase processes and liquid-phase processes. The gas evaporation method is popular because it produces nanoparticles from many kinds of materials and facilitates control over environmental conditions during the production. As an example of gas-phase processes, Ward et al. [36] produced β-Mn nanoparticles by placing a tungsten boat containing a small Mn granule inside a chamber with a support tree holding the grids directly above the sample. They found that a pure Mn nanoparticle was obtainable with a liquid nitrogen trap removing moisture content in He gas. At 40 mbar He pressure, they obtained two kinds of nanoparticles (Fig. 3), one in the size range 2–10 nm, the other in the size range 12–20 nm. The larger nanoparticles were characterized as hollow or doughnut shaped, with a thick outer edge and little or no center.

The laser ablation method involving laser irradiation toward a target, evaporation of the target material, and generation of plasma plume is another example of gas-phase processes. Nanoparticles formed in the plasma plume are deposited on a substrate in the processes. Paszti et al. [37] deposited Cu and Ag nanoparticles by

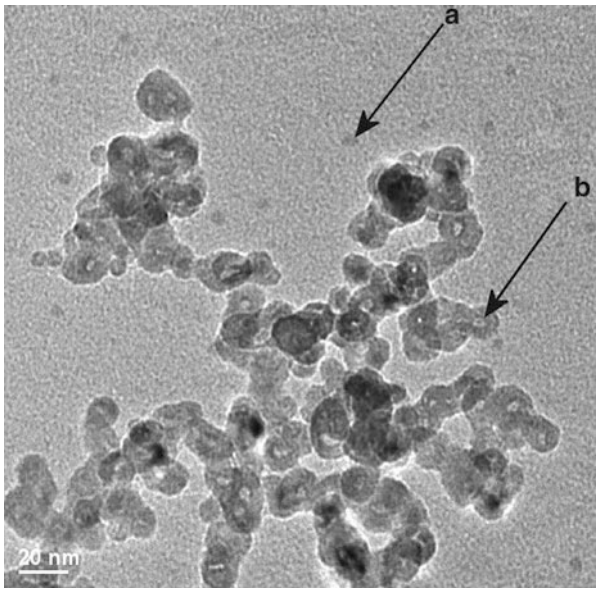

Fig. 3 A bright-field TEM image from an area of sample produced at 40 mbar He pressure. The smaller particles that fall into the size range 2–10 nm can be seen isolated across the image (*a*). The larger particles fall into the size range 12–20 nm and are formed in stringers (*b*) [36]

this process with a laser fluence of about 10 J/cm^2 in an atmosphere of up to 10 mbar Ar gas.

Kakati et al. [38] synthesized TiO_2 and TiN nanoparticles by supersonic thermal plasma expansion as one other example of gas-phase process. However, this process generally suffers from the fact that the size distribution of the nanoparticles is considerably wide. They noted that the very small residence time of the nanoparticles was a major factor to prevent coagulation of the nanoparticles in the gas phase; possible particle charging by a nonequilibrium electron population was also found to contribute toward reduction of the coagulation of nanoparticles.

For liquid-phase processes, how the initial size of nanoparticles impacts the final morphology and configuration of nanostructured materials was investigated by You et al. [39]. Aqueous $AgNO_3$ solution and zinc plate were firstly prepared, and the plate was immersed into the solution for a designed time. Ag nanostructures with different morphologies would grow on the zinc plate through the galvanic replacement reaction at different Ag ion concentrations. According to molecular dynamics calculations, stable amorphous structures appeared when the size of Ag nanoparticles was less than 2.2 nm (Fig. 4). It was clearly found that the initial size of nanoparticles performed an important role by determining the final morphology and configuration of nanostructured materials.

Magnetic nanoparticles have been of great interest because of their extensive application in areas such as high-density data storage, biochemistry, hyperthermia, and in vivo drug delivery. Their magnetic properties are size and shape dependent, and the synthesis of well-controlled shapes and sizes of magnetic nanoparticles is therefore important for their applications. Zhang et al. [40] tried to control the size

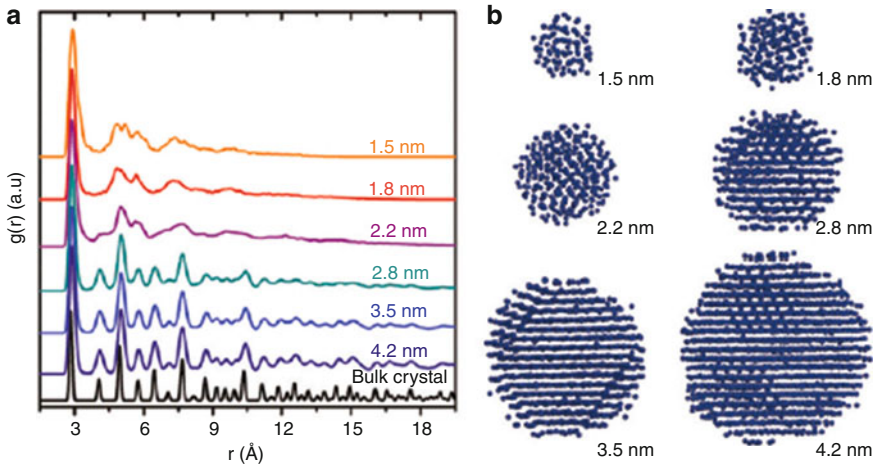

Fig. 4 Structure of computer-simulated silver NPs with different sizes in water solution: (**a**) pair correlation functions, g(r), and (**b**) structure images. The water molecules surrounding the NPs are not shown here [39]

and shape of Fe_3O_4 nanoparticles by tuning the growth reaction time in a liquid-phase process (Fig. 5).

On the other hand, Iqbal et al. synthesized nanoparticles of lanthanum calcium manganese oxide by inputting citric acid as a liquid-phase method, controlling the size and shape by tuning sintered temperature [41].

Size Effects on Physical Properties

The control of nanoparticle size is of interest because some properties of nanoparticle significantly depend on the size. For example, the melting points of nanoparticle are affected by nanoparticle size [42], as is apparent in Fig. 6. Investigating thermal properties of Na nanoparticles, Haberland et al. [43] found that the melting point and latent heat were lower than those of the bulk material for nanoparticles consisting of 135–360 atoms. Especially in the case of nanoparticles consisting of 55–340 atoms, Haberland [44] noted that the melting points were about two-thirds of the bulk melting points (in K), and both the melting points and latent heats fluctuated. There are also interesting phenomena such as premelting [43] and negative heat capacities [45].

Catalytic activity is also affected by nanoparticle size. Bulk Au is inert, whereas Au nanoparticles are very catalytically active. This size dependency has not yet been explained [46]. Joo et al. [47] investigated the effect of Ru nanoparticle size on the catalysis of CO oxidation. They found that the rate of CO oxidation catalyzed by 6 nm Ru nanoparticles was eight times than by 2 nm.

Nanoparticles are also used as electrodes of fuel cell which are possibly effective in purification of esgas products in long-duration space travel and conversion of CO

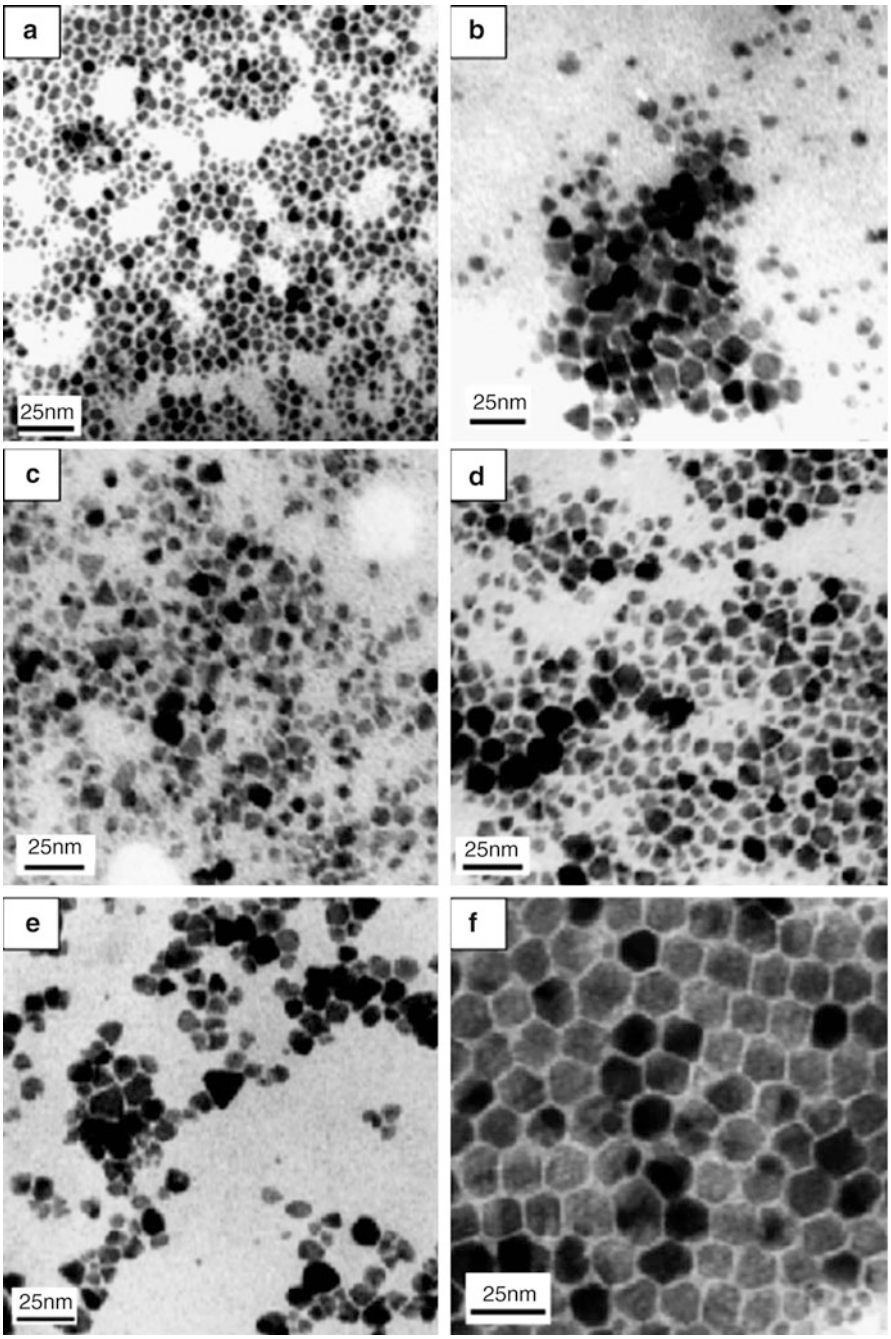

Fig. 5 TEM images of magnetite nanoparticles with different reaction stages: (**a**) seeds of 6 nm magnetite nanoparticles; (**b**) 15 min; (**c**) 30 min; (**d**) 45 min; (**e**) 60 min, after the seed-mediated growth reaction (200 °C); (**f**) 30 min after anneal treatment (300 °C) [40]

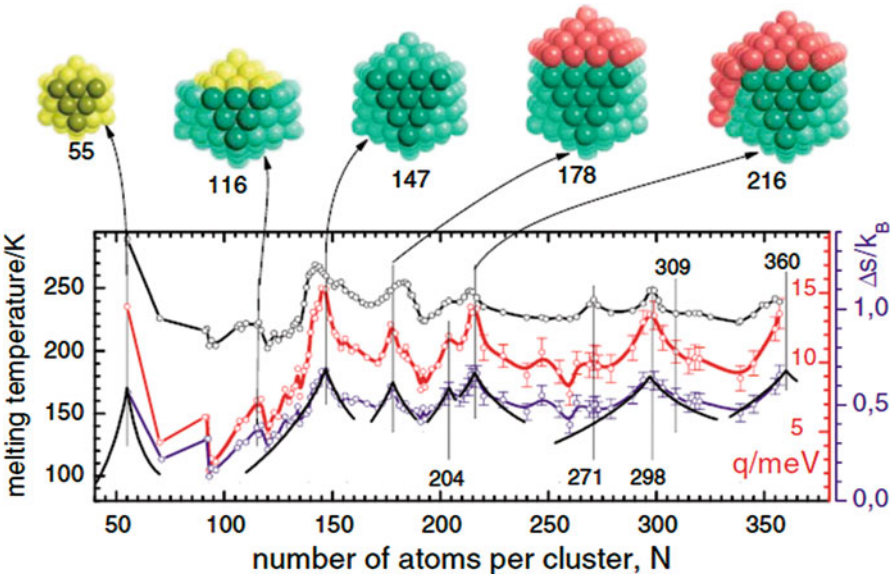

Fig. 6 Upper panel: clusters of icosahedral growth pattern. The 2nd, 3rd, and 4th layers are given in *yellow*, *green*, and *red*, respectively. One of the 20 triangular faces is colored in a deeper shade. *Lower panel*: size dependence of the melting temperature (T_{melt}, *black*), the latent heat of fusion per atom (q, *red*), and the entropy change upon melting per atom (Δs, *blue*). The data, given by the open circles, are joined (for $N > 92$) by splines. Error bars are given only for N above 200, in order to avoid cluttering the figure. The error bars for T_{melt} have about the size of the symbol used. The *black solid lines*, overlapping partially with the *blue line*, give the calculated entropy change upon melting. The simple hard sphere model gives a surprisingly good fit of the peak shapes [43]

in automobile exhaust systems. Geng et al. [48] adopted an approach employed by cyclic voltammetry to measure the activity of electrodes composed of Au nanoparticles on glassy carbon. It was found that the electrodes represented higher activity as the size of nanoparticles became smaller.

Silicon is of interest as an anode of Li batteries because it has low discharge potential and is well known to have the highest theoretical charge capacity. However, a problem specific to anode materials is the fact that performance deteriorates as a result of repeated expansions of the materials during charge–discharge cycling. To resolve the problem, Si nanowires were proposed as a novel anode instead of simple Si anode by Chan et al. [49]. They used a vapor–liquid–solid process to synthesize Si nanowires on a stainless steel substrate. Evaluation of the electrochemical properties revealed that the theoretical charge capacity for Si anodes was reached, and a discharge capacity close to 75 % at the maximum was maintained, with little fading during cycling. In theory, an improved model taking account of diffusion geometry and diffusion length distribution in nanoparticles was proposed to calculate the impedance of a Si anode by Song et al. [50].

When nanoparticles interact with photons, a localized plasmon appears due to electric charge on the surface of the nanoparticles. Applying optical Mie-plasmon

spectroscopy for Ag nanoparticles of 2 nm in average diameter, Hilger et al. [51] performed experiments which shed some light upon different aspects of these complex interfaces.

Surface Treatment of Nanoparticles

Some examples of the size effects of nanoparticles have been introduced. To educe the potential effectiveness and actually control the quality of nanoparticles, it is necessary to treat the surfaces of nanoparticles with nanocoatings. Here, the mechanism of formation of the nanocoatings and the merits of surface treatment are discussed.

Heterogeneous Nucleation

The formation of nanocoatings is described by the theory of heterogeneous nucleation. The most important parameter related to the theory is the Gibbs free energy change. Zapadinsky et al. [52] defined this parameter in the two cases: in the first case, the system contains a monomer and a substrate surface, which interacts with the monomer. This interaction is absent in the second case. In the first case, the Gibbs free energy change is defined in terms of $\Delta G_{\mathrm{hom}}(n)$ the Gibbs free energy change of an n-cluster resulting from homogeneous nucleation, as follows:

$$\Delta G_{\mathrm{het}}^{\mathrm{I}}(n) = [F_{\mathrm{het}}(n) - F_{\mathrm{hom}}(n)] - [F_{\mathrm{het}}(1) - F_{\mathrm{hom}}(1)] + \Delta G_{\mathrm{hom}}(n) \tag{29}$$

Here, the variable F denotes the Helmholtz free energy, and the subscripts het and hom represent "heterogeneous" and "homogeneous," respectively. In the latter case, $\Delta G_{\mathrm{het}}(n)$ is formulated as follows:

$$\Delta G_{\mathrm{het}}^{\mathrm{II}}(n) = [F_{\mathrm{het}}(n) - F_{\mathrm{hom}}(n)] + \Delta G_{\mathrm{hom}}(n) \tag{30}$$

Because the equilibrium concentration of an n-cluster can be predicted on the basis of a process similar to homogeneous nucleation, the heterogeneous nucleation and growth on an initial nanoparticle are understood, and the ultimate thickness of nanocoatings is successfully predicted.

Merits of Surface Treatment

As an example of nanocoatings, acrylic acid (AA) coatings on ZnO nanoparticles produced by the novel plasma treatment developed by Shi and He [53] are firstly considered. Such a coating can be used in ion exchange experiments for removal of metallic ions in water. Figure 7a–d is the bright-field images of the coated ZnO nanoparticles at various magnifications. Figure 7a, b shows a low-magnification

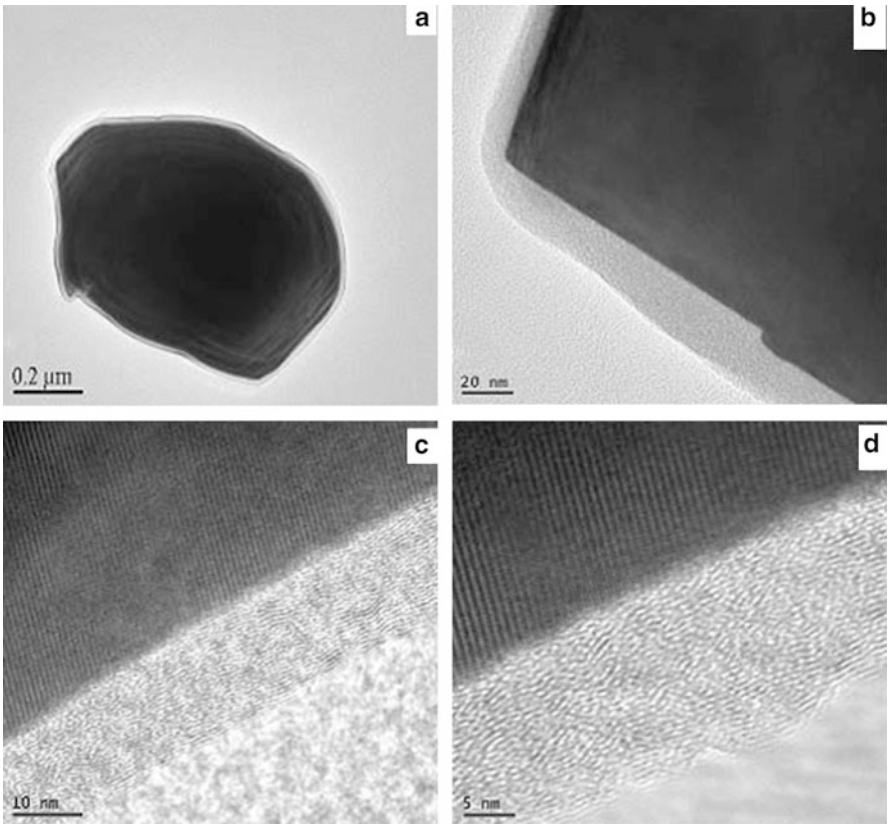

Fig. 7 (**a**) Bright-field TEM image of the AA-coated ZnO nanoparticles at low magnification. (**b**) HRTEM image showing the AA-coated ZnO nanoparticle surfaces at higher magnification. (**c**, **d**) HRTEM images of AA-coated ZnO showing the amorphous nature of the AA thin film and the crystal lattices of the ZnO structure [53]

image of a ZnO particle coated with an acrylic acid (AA) film. As can be seen, the coating is uniform over the entire surface of the particle. In the TEM image, it is apparent that although these particles had different diameters, the thickness of the films was the same, the indication being that there was a uniform distribution of active radicals in the plasma chamber. Figure 7c, d is the image at higher magnifications. The uniformity of the AA thin films can be clearly seen in these photographs. The film thickness is about 5 nm.

An example of the merits of nanocoatings is the report by Xin et al. [54], who found that the performance of a dye-sensitized solar cell fabricated from a TiO_2 nanoparticle film was much improved after the TiO_2 nanoparticle film was treated with $TiCl_4$ (Fig. 8).

Pazokifard et al. [55] evaluated silane-treated TiO_2 nanoparticles with respect to the self-cleaning properties and photoactivity of an acrylic facade coating. The

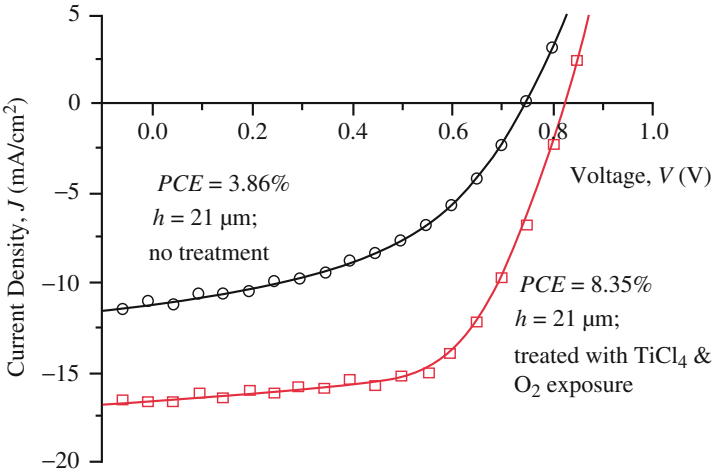

Fig. 8 J–V characteristics of DSSCs made after surface treatments with ($TiCl_4$ + O_2 plasma) and no treatment sample (Reprinted with permission from [54]. Copyright (2011) American Chemical Society). *PCE* power conversion efficiency

results showed that both the treated and untreated samples had enough photoactivity. The treated TiO_2 nanoparticles were more durable but had less activity than the untreated ones. Addition of an adequate amount of silica-treated TiO_2 nanoparticles into the acrylic coatings provided a self-cleaning property in the acrylic facade coatings.

Guo et al. [56] made a nanocomposite with alumina nanoparticles and treated the surface with (3-methacryloxypropyl)trimethoxysilane (MPS). The polymeric matrix they used was a vinyl ester resin that consisted of 55 wt% vinyl ester with an average molecular weight of 970 g mol^{-1} and 45 wt% styrene monomers. The treatment resulted in a significant increase in both modulus and strength. The addition of the functionalized nanoparticles had no deleterious effect on the thermal stability of the composite.

Hashemi-Nasab and Mirabedini [57] modified the surface of silica nanoparticles with MPS by using a two-step, sol–gel procedure. They evaluated the effects on the modifications of the surfaces of the silica nanoparticles of treatment conditions such as pH, time, and amounts of silane and water. The untreated and MPS-treated silica nanoparticles were used for in situ preparation of silica/styrene–butyl acrylate latex nanocomposites. The results showed that the treatment significantly affected the MPS grafting of nanoparticles as a result of an increase in the rate of silane hydrolysis. Furthermore, the distribution of the treated nanoparticles was better than the distribution of their untreated counterparts. Figure 9 shows TEM micrographs of untreated and MPS-treated silica nanoparticles. Kim et al. [58] used a sol–gel process to synthesize silica nanoparticles and then explored the optimum conditions for treatment of the surface of the synthesized silica nanoparticles with (3-trimethoxysilyl)propyl methacrylate (γ-MPS). After treatment of the surface

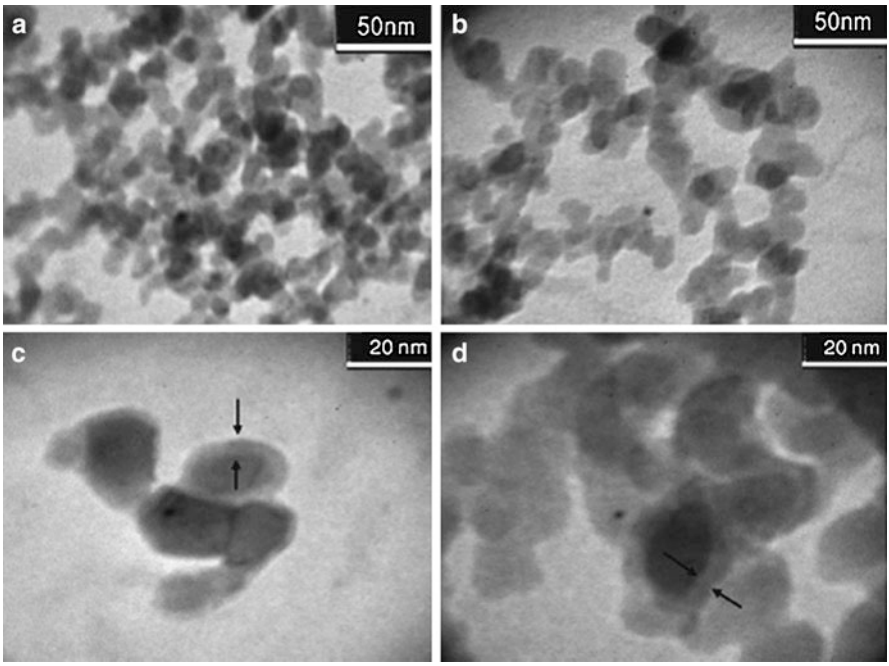

Fig. 9 TEM images of (**a**) untreated and (**b**) MPS-treated silica nanoparticles, (**c**, **d**) the thickness of silane on the silica nanoparticle surface [57]

under optimum conditions, the amount of the grafted γ-MPS per unit surface area of the silica nanoparticles was nearly the same, regardless of the particle size. Huang et al. [59] have reported that surface treatment of silica nanoparticles with (3-glycidoxypropyl) methyldiethoxysilane improved not only the dispersibility of the silica nanoparticles but also the electrical properties of the composite. These investigators say that surface treatment makes it possible to increase volume resistivity and dielectric strength and to reduce dielectric loss of composites.

Dolatzadeh et al. [60] investigated the effect of incorporation of organosilane-modified silica nanoparticles on the electrochemical behavior of the resultant coating material of polyurethane. The studies demonstrated that the modified nanoparticles were very well dispersed in the coating material and showed that the incorporation of the silica nanoparticles into the polyurethane matrix generally decreased the rate of corrosion of the coated steel substrates.

Conclusion

The dynamics of clusters as an early stage of nanoparticle formation have described, and the importance of the role of molecular partition functions has indicated in the description. Use of the molecular partition function facilitates

describing the kinetics of cluster formation without the need to distinguish between nucleation and growth, a distinction that must be made with the droplet model. During a nonequilibrium environment like a sudden gas expansion, it is actually important to consider the kinetics at the early stages of nanoparticle formation. As mentioned already, kinetic theory is also important at the initial stage of nanostructure development, which accounts for the characteristics of the secondary structure, the individual nanoparticle. In this chapter, some practical examples were introduced concerning the effects of nanoparticle size and ways of controlling the size. In addition, several studies associated with surface treatment and surface modification were discussed. These treatments were found to be imperative for increasing dispersibility in the solvent and affinity in the matrix.

References

1. G. Cao, *Nanostructures & Nanomaterials Synthesis, Properties & Applications* (Imperial College Press, London, 2004)
2. R. Kelsall, I. Hamley, M. Geoghegan, *Nanoscale Science and Technology* (Wiley, West Sussex, 2005)
3. M. Lu, H. Gong, T. Song, J.P. Wang, H.W. Zhang, T.J. Zhou, Nanoparticle composites: FePt with wide-band-gap semiconductor. J. Magn. Magn. Mater. **303**, 323–328 (2006)
4. J. Liqiang, W. Baiqi, X. Baifu, L. Shudan, S. Keying, C. Weimin, F. Honggang, Investigations on the surface modification of ZnO nanoparticle photocatalyst by depositing Pd. J. Solid State Chem. **177**, 4221–4227 (2004)
5. H. Keskinen, A. Tricoli, M. Marjamäki, M. Mäkelä Jyrki, E. Pratsinis Sotiris, Size-selected agglomerates of SnO_2 nanoparticles as gas sensors. J. Appl. Phys. **106**, 084316 (2009)
6. K. Liao, P. Mao, Y. Li, Y. Nan, F. Song, G. Wang, M. Han, A promising method for fabricating Ag nanoparticle modified nonenzyme hydrogen peroxide sensors. Sensors Actuators B Chem. **181**, 125–129 (2013)
7. B. Xie, L. Liu, X. Peng, Y. Zhang, Q. Xu, M. Zheng, T. Takiya, M. Han, Optimizing hydrogen sensing behavior by controlling the coverage in Pd nanoparticle films. J. Phys. Chem. C **115**, 16161–16166 (2011)
8. S. Ito, K. Nakaoka, M. Kawamura, K. Ui, K. Fujimoto, N. Koura, Lithium battery having a large capacity using Fe_3O_4 as a cathode material. J. Power Sources **146**, 319–322 (2005)
9. K. Kim, J.H. Park, S.G. Doo, J.D. Nam, T. Kim, Generation of size and structure controlled Si nanoparticles using pulse plasma for energy devices. Thin Solid Films **517**, 4184–4187 (2009)
10. K. Kim, J.H. Park, S.G. Doo, T. Kim, Effect of oxidation on Li-ion secondary battery with non-stoichiometric silicon oxide (SiO_x) nanoparticles generated in cold plasma. Thin Solid Films **518**, 6547–6549 (2010)
11. N.M. Strickland, N.J. Long, E.F. Talantsev, P. Hoefakker, J.A. Xia, M.W. Rupich, W. Zhang, X. Li, T. Kodenkandath, Y. Huang, Nanoparticle additions for enhanced flux pinning in YBCO HTS films. Curr. Appl. Phys. **8**, 372–375 (2008)
12. E. Ide, S. Angata, A. Hirose, K.F. Kobayashi, Metal–metal bonding process using Ag metallo-organic nanoparticles. Acta Mater. **53**, 2385–2393 (2005)
13. T. Takiya, N. Fukuda, I. Umezu, A. Sugimura, S. Ueguri, H. Yoshida, M. Han, Low temperature bonding of metals by deposition of nanoparticles at the interface. Appl. Phys. Res. **4**, 42–47 (2012)
14. K. Wegner, P. Piseri, H.V. Tafreshi, P. Milani, Cluster beam deposition: a tool for nanoscale science and technology. J. Phys. D. Appl. Phys. **39**, R439–R459 (2006)

15. Z.H. Wang, D.Y. Geng, Z. Han, Z.D. Zhang, Large critical magnetic field and tunneling anomaly behavior of superconducting carbon-coated Sn nanorods and nanoparticles. J. Appl. Phys. **108**, 013903 (2010)
16. S. He, Y. Jing, J.P. Wang, Direct synthesis of large size ferromagnetic $SmCo_5$ nanoparticles by a gas-phase condensation method. J. Appl. Phys. **113**, 134310 (2013)
17. L. He, X. Chen, Y. Mu, F. Song, M. Han, Two-dimensional gradient Ag nanoparticle assemblies: multiscale fabrication and SERS applications. Nanotechnology **21**, 495601 (2010)
18. S. Lee, H.F. Chen, C.J. Chin, Spectroscopic study of carbonaceous dust particles grown in benzene plasma. J. Appl. Phys. **101**, 113303 (2007)
19. E.G. Gamaly, N.R. Madsen, D. Golberg, A.V. Rode, Expansion-limited aggregation of nanoclusters in a single-pulse laser-produced plume. Phys. Rev. B **80**, 184113 (2009)
20. M. Nagashima, T. Takiya, S. Furuta, H. Yoshida, Y. Oda, K. Ichimori, S. Ueguri, Fabrication and characterization of ZrO_2-Al_2O_3 films using pulsed laser ablation, in *International conference on electronic materials and nanotechnology for green environment*, Jeju Island, 21–24 Nov 2010
21. T. Takiya, N. Fukuda, N. Inoue, M. Han, M. Yaga, Y. Iwata, Dynamics of the shock wave accompanied by nanoparticle formation in the PLA processes. Adv. Stud. Theor. Phys. **4**, 305–316 (2010)
22. K. Petcharoena, A. Sirivat, Synthesis and characterization of magnetite nanoparticles via the chemical co-precipitation method. Mater. Sci. Eng. B **177**, 421–427 (2012)
23. IA. Rahman, V. Padavettan, Synthesis of silica nanoparticles by sol–gel: size-dependent properties, surface modification, and applications in silica polymer nanocomposites – a review. J. Nanomater., Volume 2012, ID132424, 1–15(2012)
24. A. Tabrizi, F. Ayhan, H. Ayhan, Gold nanoparticle synthesis and characterisation. Hacet. J. Biol. Chem. **37**, 217–226 (2009)
25. T.T.Q. Hoa, L.V. Vu, T.D. Canh, N.N. Long, Preparation of ZnS nanoparticles by hydrothermal method. J. Phys. Conf. Ser. **187**, 012081 (2009)
26. T. Takiya, M. Han, M. Yaga, Thermodynamics of nanoparticle formation in laser ablation, in *Thermodynamics Interaction Studies-Solids, Liquids and Gases*, ed. by J.C. Moreno-Pirajan (InTech, Rijeka, 2011), pp. 123–146
27. P.G. Hill, Condensation of water vapour during supersonic expansion in nozzles. J. Fluid Mech. **25**, 593–620 (1966)
28. J. Feder, K.C. Russell, J. Lothe, G.M. Pound, Homogeneous nucleation and growth of droplets in vapours. Adv. Phys. **15**, 111–178 (1966)
29. G.K. Schenter, S.M. Kathmann, B.C. Garrett, Dynamical nucleation theory: a new molecular approach to vapor–liquid nucleation. Phys. Rev. Lett. **82**, 3484–3487 (1999)
30. H.P. Godfried, I.F. Silvere, Raman studies of argon dimers in a supersonic expansion. II. Kinetics of dimer formation. Phys. Rev. A **27**, 3019–3030 (1982)
31. B.K. Rao, B.M. Smirnov, Cluster growth in expanding copper vapor. Mater. Phys. Mech. **5**, 1–10 (2002)
32. R.B. McClurg, R.C. Flagan, Critical comparison of droplet models in homogeneous nucleation theory. J. Colloid Interface Sci. **201**, 194–199 (1998)
33. D. Kashchiev, *Nucleation: Basic Theory with Applications* (Butterworth-Heinemann/Elsevier, Oxford, 2000)
34. H. Eyring, The activated complex in chemical reactions. J. Chem. Phys. **3**, 107 (1935)
35. R. Zhang, A. Khalizov, L. Wang, M. Hu, W. Xu, Nucleation and growth of nanoparticles in the atmosphere. Chem. Rev. **112**, 1957–2011 (2012)
36. M.B. Ward, R. Brydson, R.F. Cochrane, Mn nanoparticles produced by inert gas condensation. J. Phys. Conf. Ser. **26**, 296–299 (2006)
37. Z. Pászti, Z.E. Horváth, G. Petõ, A. Karacs, L. Guczi, Pressure dependent formation of small Cu and Ag particles during laser ablation. Appl. Surf. Sci. **109–110**, 67–73 (1997)
38. M. Kakati, B. Bora, S. Sarma, B.J. Saikia, T. Shripathi, U. Deshpande, A. Dubey, G. Ghosh, A.K. Das, Synthesis of titanium oxide and titanium nitride nano-particles with narrow size distribution by supersonic thermal plasma expansion. Vacuum **82**, 833–841 (2008)

39. H. You, F. Chen, S. Yang, Z. Yang, B. Ding, S. Liang, X. Song, Size effect on nanoparticle-mediated silver crystal growth. Cryst. Growth Des. **11**, 5449–5456 (2011)
40. L. Zhang, R. He, H.C. Gu, Synthesis and kinetic shape and size evolution of magnetite nanoparticles. Mater. Res. Bull. **41**, 260–267 (2006)
41. M.Z. Iqbal, S. Ali, M.A. Mirza, Effect of particle size on the structural and transport properties of $La_{0.67}Ca_{0.33}MnO_3$ nanoparticles. CODEN JNSMAC **48**, 51–63 (2008)
42. M. Schmidt, J. Donges, T. Hippler, H. Haberland, Influence of energy and entropy on the melting of sodium clusters. Phys. Rev. Lett. **90**, 103401 (2003)
43. H. Haberland, T. Hippler, J. Donges, O. Kostko, M. Schmidt, B. von Issendorff, Melting of sodium clusters: where do the magic numbers come from? Phys. Rev. Lett. **94**, 035701 (2005)
44. H. Haberland, Melting of clusters, in *Atomic Clusters and Nanoparticles Les Houches Session LXXIII 2–28 July 2000*, ed. by C. Guet. Les Houches – Ecole d'Ete de Physique Theorique, vol. 73 (Springer, Heidelberg, 2001), pp. 29–56
45. M.D. Agostino, F. Gulminelli, P. Chomaz, M. Bruno, F. Cannata, R. Bougault, F. Gramegna, I. Iori, N. Le Neindre, G.V. Margagliotti, A. Moroni, G. Vannini, Negative heat capacity in the critical region of nuclear fragmentation: an experimental evidence of the liquid–gas phase transition. Phys. Lett. B **473**, 219–225 (2000)
46. B.R. Cuenya, Synthesis and catalytic properties of metal nanoparticles: size, shape, support, composition, and oxidation state effects. Thin Solid Films **518**, 3127–3150 (2010)
47. S.H. Joo, J.Y. Park, J.R. Renzas, D.R. Butcher, W. Huang, G.A. Somorjai, Size effect of ruthenium nanoparticles in catalytic carbon monoxide oxidation. Nano Lett. **10**, 2709–2713 (2010)
48. D. Geng, G. Lu, Size effect of gold nanoparticles on the electrocatalytic oxidation of carbon monoxide in alkaline solution. J. Nanoparticle Res. **9**, 1145–1151 (2007)
49. C.K. Chan, H. Peng, G. Liu, K. McIlwrath, X.F. Zhang, R.A. Huggings, Y. Cui, High-performance lithium battery anodes using silicon nanowires. Nat. Nanotechnol. **3**, 31–35 (2008)
50. J. Song, M.Z. Bazant, Effects of nanoparticle geometry and size distribution on diffusion impedance of battery electrodes. J. Electrochem. Soc. **160**, A15–A24 (2013)
51. A. Hilger, T. von Hofe, U. Kreibig, Recent investigations of size and interface effects in nanoparticle composites. Nova Acta Leopold. Neue Folge **92**, 9–19 (2005)
52. E. Zapadinsky, A. Lauri, M. Kulmala, The molecular approach to heterogeneous nucleation. J. Chem. Phys. **122**, 114709 (2005)
53. D. Shi, P. He, Surface modifications of nanoparticles and nanotubes by plasma polymerization. Rev. Adv. Mater. Sci. **7**, 97–107 (2004)
54. X. Xin, M. Scheiner, M. Ye, Z. Lin, Surface-treated TiO_2 nanoparticles for dye-sensitized solar cells with remarkably enhanced performance. Langmuir **27**, 14594–14598 (2011)
55. S. Pazokifard, M. Esfandeh, S.M. Mirabedini, M. Mohseni, Z. Ranjbar, Investigating the role of surface treated titanium dioxide nanoparticles on self-cleaning behavior of an acrylic facade coating. J. Coat. Technol. Res. **10**, 175–187 (2013)
56. Z. Guo, T. Pereira, O. Choi, Y. Wang, H.T. Hahn, Surface functionalized alumina nanoparticle filled polymeric nanocomposites with enhanced mechanical properties. J. Mater. Chem. **16**, 2800–2808 (2006)
57. R. Hashemi-Nasab, S.M. Mirabedini, Effect of silica nanoparticles surface treatment on in situ polymerization of styrene–butyl acrylate latex. Prog. Org. Coat. **76**, 1016–1023 (2013)
58. J.W. Kim, L.U. Kim, C.K. Kim, Size control of silica nanoparticles and their surface treatment for fabrication of dental nanocomposites. Biomacromolecules **8**, 215–222 (2007)
59. X. Huang, Y. Zheng, P. Jiang, Influence of nanoparticle surface treatment on the electrical properties of cycloaliphatic epoxy nanocomposites. IEEE Trans. Dielectr. Electr. Insul. Soc. **17**, 635–643 (2010)
60. F. Dolatzadeh, S. Moradian, M. Mehdi Jalili, Influence of various surface treated silica nanoparticles on the electrochemical properties of SiO_2/polyurethane nanocoatings. Corros. Sci. **53**, 4248–4257 (2011)